Annals of Biomedical Engineering
https://doi.org/10.1007/s10439-026-04121-w

BMES BIOMEDICAL ENGINEERING SOCIETY

ORIGINAL ARTICLE

Passive Mechanical Testing of Female Human Levator Ani and Superficial Perineal Muscles

Megan R. Routzong[1,2,3] · Justin Dubik[4] · Raffaella De Vita[4] · Marianna Alperin[2,5] · Pamela A. Moalli[1,6] · Steven D. Abramowitch[1]

Received: 7 August 2025 / Accepted: 25 March 2026

Abstract

The levator ani muscles (LAMs) and superficial perineal muscles (SPMs) are critical to pelvic organ support. While few studies have investigated the female human LAMs via ex vivo mechanical testing, even fewer have investigated the SPMs. In this study, we evaluated female human LAMs and SPMs via ex vivo uniaxial tensile testing, hypothesizing that the LA would have a distinct response compared to the SPMs. SPM—bulbocavernosus (BC), ischiocavernosus (IS), transverse perinei (TP)—and LAM samples were obtained from 8 fresh-frozen female human cadavers. LAMs and SPMs were dissected en bloc as a pelvic floor complex, stored frozen, and then individual muscle specimens were dissected from thawed complexes for mechanical testing. Extension-to-failure tests were performed at a displacement rate of 5 mm min^{-1}, strains were measured using digital image correlation, and load–displacement and stress–strain curves (axial and transverse) were generated. The LAMs exhibited the most compliant behavior, divergent from that of the SPMs, while the IS demonstrated the stiffest response on average. Though SPMs were more similar to one another than to the LAMs, average stress–axial strain curves distinguished between individual SPMs. These results support our hypothesis that the passive mechanical behavior of the LAMs is distinct from that of the SPMs, suggesting it is inappropriate to use LAM material properties to describe SPMs. Additionally, distinction between stress–axial strain curves suggests muscle-specific mechanical properties should be considered even within the SPMs. This study provides novel data critical to improving our understanding of female human LAMs and SPMs and our ability to accurately simulate them and motivates future studies to further investigate their mechanical properties.

Keywords Ex vivo uniaxial mechanical testing · Female pelvic floor · Levator ani muscles · Superficial perineal muscles

Associate Editor Joel Stitzel oversaw review of this article.

✉ Megan R. Routzong
mer136@pitt.edu

[1] Department of Bioengineering, University of Pittsburgh, Pittsburgh, PA, USA

[2] Department of Obstetrics, Gynecology & Reproductive Sciences, University of California San Diego, La Jolla, CA, USA

[3] Departments of Biomedical Engineering and Obstetrics & Gynecology, University of Texas Southwestern Medical Center, Dallas, TX, USA

[4] STRETCH Lab, Department of Mechanical Engineering, Virginia Tech, Blacksburg, VA, USA

[5] Sanford Consortium for Regenerative Medicine, La Jolla, CA, USA

[6] Department of Obstetrics, Gynecology & Reproductive Sciences, University of Pittsburgh, Pittsburgh, PA, USA

Introduction

The skeletal muscles that span the pelvic outlet, collectively referred to as pelvic floor muscles, provide important mechanical support to the pelvic organs. The pelvic floor muscles play a crucial role in the physiological functions of the pelvic floor, such as urination, defecation, and sexual function, for all individuals. However, women in particular may experience critical life events that expose the pelvis and pelvic floor to unique and extreme loading conditions. Studies have shown that pregnancy induces pelvic floor muscle remodeling [1–5], while vaginal delivery has been shown to frequently cause acute injury that increases the risk of pelvic floor muscle dysfunction later in life [6–10]. Pelvic floor muscle dysfunction or injury predisposes women to pelvic floor disorders, which include conditions such as urinary incontinence, fecal incontinence, and pelvic organ

Published online: 18 April 2026

prolapse. Pelvic floor disorders are common, particularly in older, parous, and postmenopausal women, and affect approximately one third of adult women [11].

Despite the functional importance of the pelvic floor muscles and their high rate of injury/dysfunction, little is known about their material properties or mechanical behavior. Human levator ani muscles (LAMs), which span the pelvic outlet and form the hiatus that the pelvic organs pass through, have been mechanically tested ex vivo [12, 13], but these studies are few. The superficial perineal muscles (SPMs) are superficial to the LAMs, surround the openings of the urethra and vagina, and interface with the perineal body that lies between the vaginal introitus and anus [14]. Although much smaller than the LAMs, the mechanical behavior of the SPMs is also likely important to pelvic organ function. The SPMs, along with the LAMs, contribute to Level III vaginal support (a term to define structures that directly impact mechanical support to the lower third of the vagina) [15] and their inclusion in computational models has been shown to significantly influence simulations of vaginal childbirth, specifically during fetal head crowning [16, 17]. If SPM mechanical behavior cannot be accurately approximated by existing LAM mechanical properties, then the accuracy of resulting simulations and model predictions (e.g., stress, injury, etc.) are at risk, limiting their efficacy and potential future clinical translation. This has potential implications for any models simulating the biomechanics of the female pelvic floor, but particularly those involving vaginal childbirth, injury prediction, and recovery/treatment after injury or the development of pelvic floor dysfunction. Thus, it is important to study the mechanical behavior of both the LAMs and SPMs to inform future simulations of the female pelvic floor.

In this study, we aimed to characterize the passive mechanical behavior of human female LAMs and SPMs via ex vivo mechanical testing of cadaveric specimens. Due to known differences in their morphology and mechanical environment in vivo, we hypothesized that the LAMs would exhibit behavior distinct from that of the SPMs.

Materials and Methods

En bloc Pelvic Floor Dissection

Pelvic floor tissues were dissected from consented/authorized female human cadaver donors procured through the Anatomy Gifts Registry, a licensed and accredited whole body donation program, with approval from the Committee for Oversight of Research and Clinical Training Involving Decedents (CORID) at the University of Pittsburgh. Inclusion criteria required the donor to be at least 18 years of age, female, and the pelvis to include the urethra, vagina, and rectum. Exclusion criteria included a history of pelvic floor repair/reconstruction surgery or pelvic cancer. Notably, inclusion/exclusion criteria did not include demographic or medical history variables such as parity, Cesarean section or related scars, hysterectomy/presence of uterus/cervix, donor age, weight, menopausal status, cause of death, level of physical activity, etc.

Fresh-frozen cadaveric torsos (either full torso or L4/5 to mid-femur) arrived frozen. Thawing required approximately 3 days at room temperature. The full dissection of each en bloc pelvic floor complex was carried out following the same 4 general steps: (1) Exposure of the SPMs and connective tissues; (2) exposure of the external anal sphincter and the posterior surface of the LAMs; (3) pelvic evisceration with removal of the deeper portions of the urethra, vagina, and rectum, and (4) detachment of the en bloc pelvic floor complex from the bony pelvis. Each excised complex most notably included the LAMs, SPMs, clitoris, and the most superficial portions of the urethra, vagina, and rectum.

Dissections began by exposing the SPMs and superficial connective tissues (such as the perineal body) with the cadaveric torso in the supine position. Initial incisions were made on the anterior side of the pubic symphysis. The suspensory ligament of the clitoris was located and exposed, following the structure down its length toward its inferior insertion onto the clitoris. The portions of the left and right ischiocavernosus and bulbocavernosus muscles closest to the body of the clitoris were located and exposed. To fully expose the bulbocavernosus, it was followed from the clitoris laterally around the external urethral meatus and vaginal introitus to the perineal body. To fully expose the ischiocavernosus, it was followed laterally down the ischiopubic rami toward the insertion of the superficial transverse perinei onto the ischial tuberosity. This revealed the plane in which the perineal body, deep and superficial transverse perinei, and the anterior portion of the external anal sphincter could be viewed.

The torso was then placed in the prone position for the posterior portion of the dissection. The plane of dissection identified by exposing the SPMs and connective tissues was followed posteriorly toward the coccyx, exposing the rest of the external anal sphincter. Once the surface of the external anal sphincter was fully visible, the annococcygeal ligament was located at its insertion on the posterior surface of the external anal sphincter and followed to its attachment to the coccyx. The posterior surface of the LAMs was exposed by removing portions of the gluteus maximums muscles and as much adipose tissue as possible from the ischiorectal fossa. The sacrospinous ligaments were used to locate the superior edges of the LAMs during this process.

The torso was then returned to the supine position to expose the ventral/medial surfaces of the LAMs. An abdominal incision was used to reveal and then remove the pelvic

viscera, only leaving the most distal segments (approximately 3 cm in length) of the urethra, vagina, and rectum as not to disturb the LAMs and SPMs in those regions. Notably, this involved detaching the rectum from the ventral surface of the posterior LAMs by cutting away fascia. The vagina was detached from the ventral surface of each lateral wall of the LAMs by severing the tissues providing level I and II vaginal support.

Finally, both dorsal and ventral approaches were used to detach the LAMs from the bony pelvis and pelvic sidewalls. This involved separating them from the obturator internus along the arcus tendineus levator ani. The SPMs were detached from the ischiopubic rami with the torso in the supine position. Then, the pelvic floor complex was removed en bloc and a brief amount of time was taken to remove remaining adipose and extraneous tissues.

Each en bloc pelvic floor complex was wrapped in saline soaked gauze, stored in double bagged resealable plastic bags, and frozen at −20 °C. Complexes were frozen en bloc to save time and more easily maintain in vivo orientations until mechanical testing. Because the dissection of the pelvic floor complex was already so time-consuming, it was decided that leaving the tissues at room temperature long enough for consecutive individual muscle dissections risked compromising their integrity.

Individual Muscle Dissections

En bloc pelvic floor complexes remained frozen until two days prior to mechanical testing, when they were moved to a 4 °C refrigerator to thaw. They finished thawing at room temperature immediately prior to individual muscle dissection. During and following these dissections and leading up to mechanical testing, dissected muscles and complexes were kept hydrated by periodically spraying them with 1× phosphate-buffered saline.

Individual muscles were isolated from each en bloc pelvic floor complex (Fig. 1). These muscle specimens included left and right ischiocavernosus (IS), bulbocavernosus (BC), transverse perinei (TP, sometimes both deep and superficial) muscles, and the pubovisceral and iliococcgeus subdivisions of the LAMs. Due to size and shape with respect to the mechanical testing clamps, LAM specimens could not be tested whole. They were divided into sections by cutting with the orientation of the muscle fascicles and between them, using natural gaps between fascicles when present (e.g.,

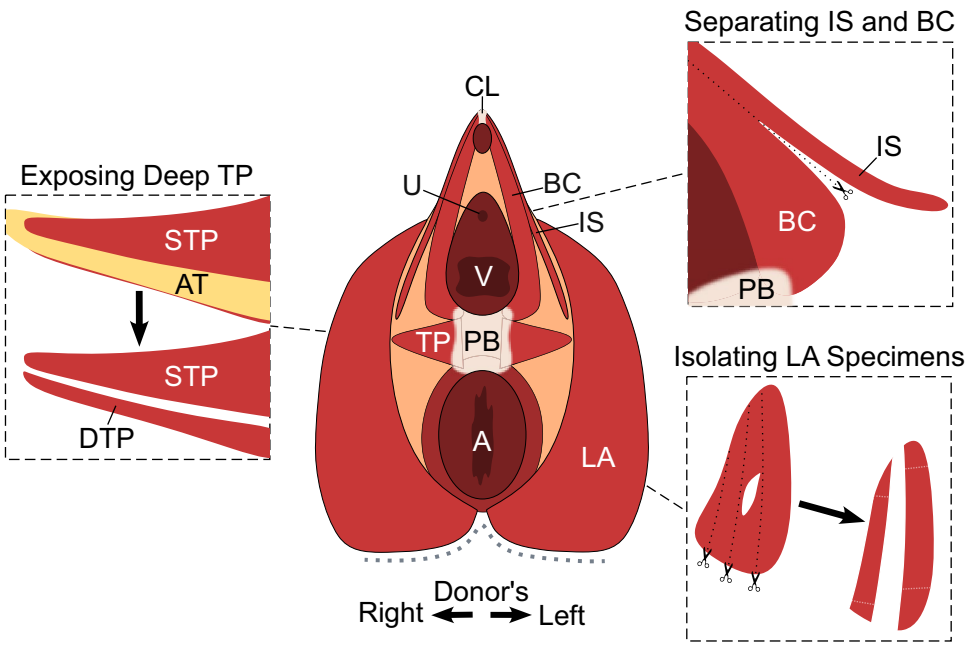

Fig. 1 An illustration of an excised, intact pelvic floor complex from an anatomically inferior perspective as it would appear if placed on a table with the more superficial surfaces facing upward. The anterior side of the complex is oriented toward the top of this illustration, where the clitoral ligament (CL) is located, and the posterior side is oriented toward the bottom of the illustration, where the aponeurosis joining the left and right levator ani was cut (the edge denoted by the gray-dotted line) to allow these muscles to lie as flat as possible in frozen storage. The call-out boxes describe specific steps of the individual muscle dissection process: **Top Right**) Separation of the ischiocavernosus (IS) from the bulbocavernosus (BC), **Left**) exposure of the deep transverse perinei (DTP) located beneath the superficial transverse perinei (STP) and a layer of adipose tissue (AT), and **Bottom Right**) division of the levator ani (LA) into individual mechanical testing specimens. Arrows point from before to after when denoting dissection steps, dotted lines with scissors indicate where cuts were made, and dotted white lines (in the LA call-out box) represent where specimens would have been clamped for mechanical testing. The urethra (U), vagina (V), perineal body (PB), and anus (A) are also denoted.

pockets of adipose or connective tissue) to create specimens of reasonable testing size while minimizing variations in width along the length of each specimen. This resulted in visible muscle fascicles being closely aligned with the central axis of each specimen's length. This always needed to be done for the LAM samples, which were too wide to be tested whole. Thus, most LAM samples generated multiple mechanical testing specimens, even when considering the left and right sides individually. Additionally, this meant that the region from which LAM specimens were obtained varied more than it could for any of the SPMs (which could usually be tested nearly whole) and could have come from either the pubovisceralis or iliococcygeus (Fig. 2). Due to difficulties in identifying all LAM subdivision borders from excised pelvic floor complexes and the fact that Burnett et al. did not find differences in the passive mechanics between the pubovisceralis and iliococcygeus at the bundle level, LAM specimens were grouped together rather than by individual muscles [12]. Regarding the SPMs, for just a few samples, the medial edge of the TP muscle was too broad. In such cases, that edge was trimmed, cutting between muscle fascicles just enough for its width to be encompassed by the clamp. Additionally, for the TP specifically, there were instances where distinct superficial and deep layers of muscle separated by adipose tissue were identified. If each could be dissected without damaging the other, both deep and superficial samples were dissected and tested. However, in most cases, only superficial TP muscles could be identified and dissected. In general, SPM specimens did not require trimming prior to mechanical testing.

Specimen Preparation

Following dissection, specimens were moved to a 10 cm labeled culture dish where muscle fascicle orientations and hydration could be maintained. This ensured that specimens' muscle fibers would be aligned as parallel as possible to the primary loading axis during uniaxial mechanical testing. Thicknesses and widths were measured perpendicular to the primary orientation of clearly visible muscle fascicles at three different points along the length of each specimen (near each end and in the middle). The locations of the mechanical testing clamps were approximated and an attempt was made not to take width and thickness measurements at locations that would be clamped during mechanical testing. The widths were measured via digital calipers (accuracy ± 0.05 mm, Mitutoyo ABSOLUTE Digimatic Low Force Caliper, Kawasaki, Japan) and thicknesses via a CCD laser displacement sensor (LK-G82, Keyence Inc., Japan). Thickness was measured along the approximate

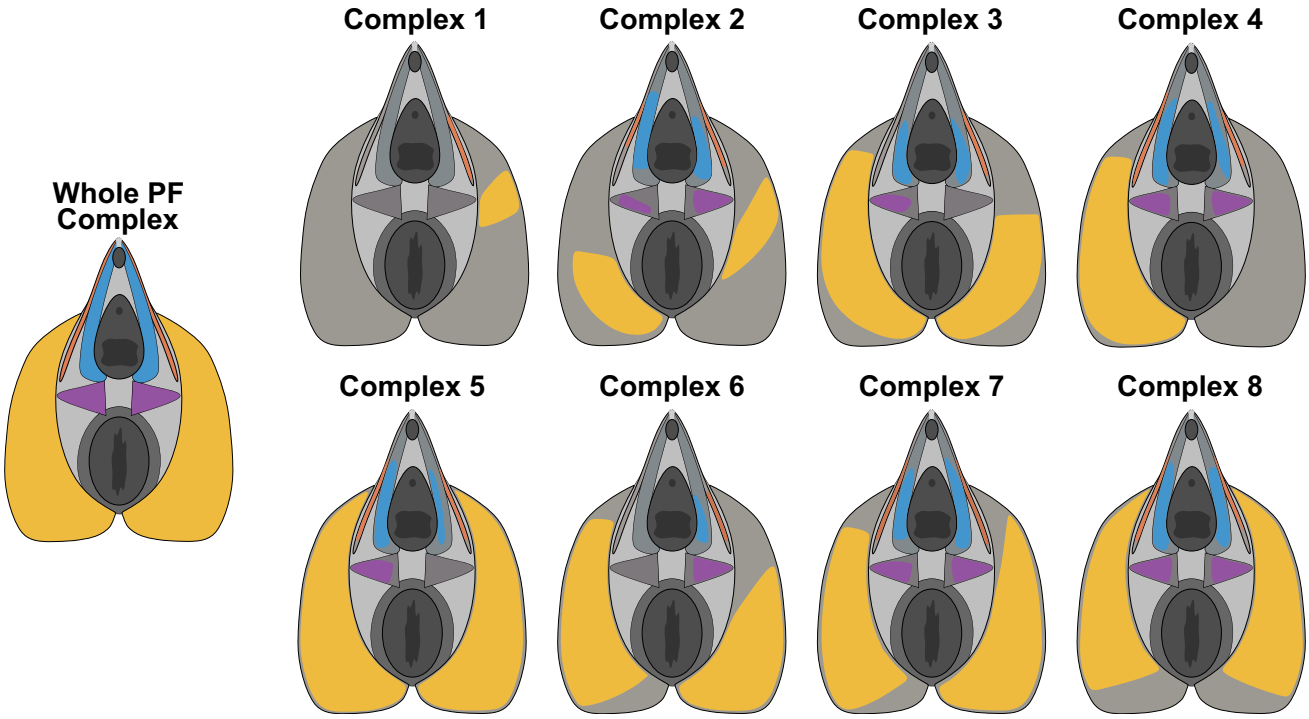

Fig. 2 Approximate regions from which mechanical testing specimens were isolated from excised pelvic floor (PF) complexes. Areas depicted in color represent the region from which the mechanical testing specimen(s) were obtained. The PF complex to the left represents a whole complex and serves as a legend in subsequent figures. The ischiocavernosus muscles are shown in red, the bulbocavernosus in blue, the transverse perinei in purple, and the levator ani in yellow.

center axis of the specimen. Muscle specimens were then dyed blue with a 1% methylene blue solution (Fisher Science Education, Nazareth, PA, USA) and sprayed with white spray paint (Rust-Oleum, Vernon Hills, IL, USA) to produce a high contrast speckle pattern for local non-contact strain measurement during mechanical testing [18].

Uniaxial Mechanical Testing

Muscle specimens were mounted via tensile grips into a uniaxial tensile testing system (ElectroPuls E1000, Instron, Norwood, MA) equipped with a 50 N load cell (±0.05 N, Instron, Norwood, MA). To prevent slippage, each end of the specimen was pinched in a wedge of sandpaper similar in length and width to the wedge action tensile grips of the testing system. One pinched edge was brought to the top clamp and secured in place. Then, the sample's position was adjusted until the bottom edge pinched in sandpaper was aligned to the bottom clamp. That end was also secured in the clamp and the sample's top end adjusted until the force was nearly zero. Gauge length between clamps was measured via digital calipers (accuracy ± 0.2 mm, Mitutoyo ABSOLUTE Digimatic Caliper Series 500, Kawasaki, Japan). Given the paucity of existing data, it was decided that a simple protocol would be implemented. Specimens were preloaded to 0.1 N at a displacement rate of 1 mm min^{-1}. Uniaxial tensile testing was then performed at a displacement rate of 5 mm min^{-1} while measuring load and displacement at a sampling rate of at least 10 Hz. Concurrently, two CCD cameras (Basler ace acA2440-75 μm, Basler Inc., Exton, PA) captured high-resolution images of each specimen at a rate of 2 Hz for 3D digital image correlation (DIC) strain measurements (Fig. 3). Testing was conducted until failure of the specimen (i.e., tearing in the midsection resulting in sustained loss of force) or clamp failure (i.e., slipping or tearing of the specimen from or at the edge of the clamp resulting in sustained loss of force or sustained force with increasing clamp displacement). As it would hinder DIC strain measurement, samples were not hydrated during mechanical testing.

Data Analysis

Force and extension data were recorded by the tensile testing system. The average of the three widths and thicknesses measured prior to testing were used to calculate each specimen's initial cross-sectional area. Nominal (i.e., engineering) axial stress throughout testing was calculated by dividing the recorded load by the initial cross-sectional area and, though it differs from true stress, is a widely accepted output for uniaxial tensile testing of biological tissues [19, 20].

Continuous load–displacement curves were generated for each specimen and trimmed to remove data that may

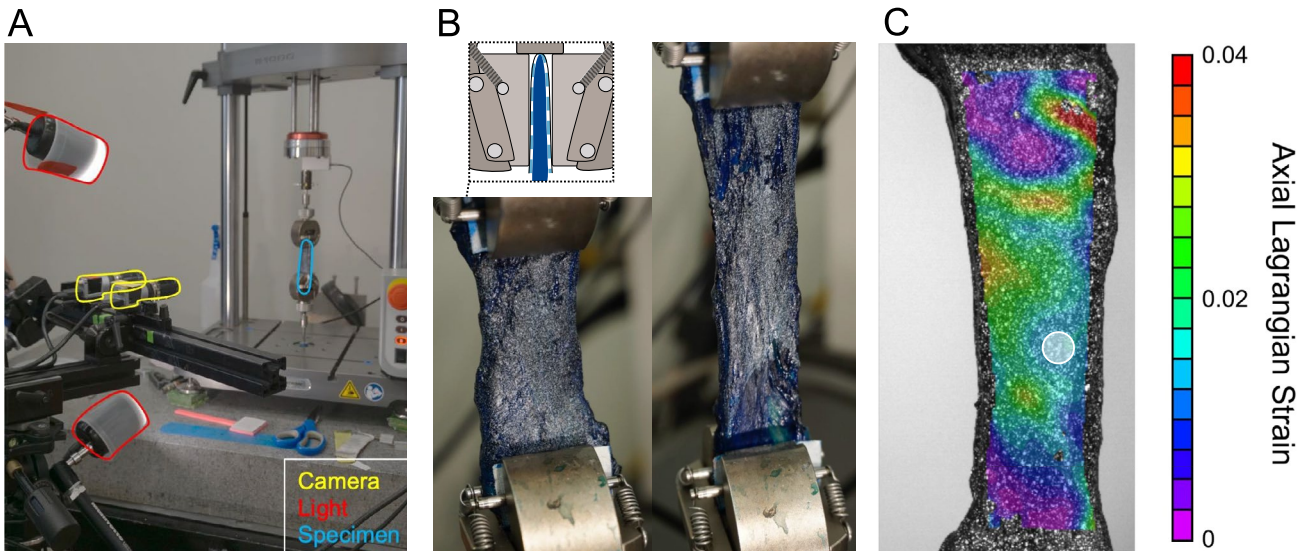

Fig. 3 An overview of our mechanical testing approach and digital image correlation (DIC) based analyses. **A** The uniaxial mechanical testing equipment and DIC-associated accessories used in this study. Each CCD camera is outlined in yellow, each diffuse light source is outlined in red, and the specimen secured with sandpaper within the clamps is outlined in blue. **B** One levator ani (LA) specimen immediately before (left) and during (right) uniaxial mechanical testing. A call-out box visualizes the left side of the clamp and how wedges of sandpaper (depicted as light blue and white) encompassed the ends of each specimen (depicted as dark blue). **C**) An example of a DIC strain map at one point in time across the portion of the specimen within the field of view. The white circle is the region of interest (ROI) used to calculate average strain for that specimen.

have been recorded after specimen or clamp failure. Thus, failure loads/displacements were not included in this analysis. As 18 of 63 specimens experienced clamp failure, comparisons of failure loads/displacements would not have been meaningful. Average curves were generated for each muscle group. However, obviously, not all specimens reached the same maximum displacement. To prevent sudden changes in average values resulting from specimen failure or slippage with increasing displacement, only data from specimens that reached a displacement of at least 16 mm were used to calculate these average curves. This value was chosen as it was the largest discrete displacement where each muscle group retained an $N \geq 3$. To allow for the comparison of all data regardless of the ultimate load or displacement values, individual load–displacement curves were sampled at discrete displacement values (from 2 mm to 42 mm at 2 mm increments) to generate discrete load–displacement plots.

Local heterogeneous Lagrangian strain fields were calculated using a DIC system (Vic-3D 9, Correlated Solutions, Columbia, SC) that was calibrated via imaging of a 14 × 10 dot calibration grid with 3 mm spacing. While camera positions and settings may have been adjusted as needed to improve visual clarity for optimal data collection of each specimen, these adjustments were minor (convergence angles and working distances were always similar) and each setup was recalibrated to the same grid. For data processing, large subset sizes (>60 pixels) minimized strain noise and small step sizes (<10 pixels) maximized spatial resolution, though values varied to mitigate loss of data locally on the surface of each sample. These acquisition and post-processing approaches ensured that the DIC strain measurements were consistent and reliable. For each specimen, a small circular sub-region (diameter < 2 mm) was selected based on the best speckle visibility and how long the region remained within the field of view of the cameras. When possible, this region was selected to be away from the clamped ends, near the center of the specimen, and distanced from local concentrations in strain (Fig. 3C). From this sub-region, the average normal Lagrangian strains were calculated for each image recorded during testing, taken as the representative strains for that specimen. Both axial (i.e., parallel to the main in vivo loading direction and most muscle fibers) and transverse (i.e., perpendicular to the main loading direction and most muscle fibers) Lagrangian strains were calculated.

Strain data from DIC and load and displacement data from the tensile testing system were aligned and noise reduced with a custom MATLAB script (R2023a, Mathworks, Natick, MA). As with the load–displacement analysis, continuous stress–strain (axial and transverse) curves were also generated for each specimen and trimmed in a similar manner. However, sometimes DIC data could not be obtained for the end portion of a test due to the sub-region leaving the field of view or the software's inability to continue to detect the speckle pattern, and, thus, calculate strain. Therefore, some stress–strain curves were trimmed to an earlier time point than the corresponding load–displacement data. Additionally, in some cases, DIC data could not be successfully obtained when load–displacement data could. Thus, sample sizes for the load–displacement data are greater than those for the stress–strain data.

Average stress–strain (axial and transverse) curves for each muscle group were also generated using data from specimens that reached an ultimate stress of at least 0.06 MPa. This value was chosen as it was the largest discrete stress where each muscle group retained an $N \geq 3$. To account for all data regardless of ultimate/final stress–strain values, individual stress–strain curves were sampled at specified stress values to generate discrete stress–strain data [21]. To capture the approximate toe regions for these specimens, curves were sampled between 0.002 and 0.020 MPa at an increment of 0.002 MPa. To capture the approximate linear regions, stress–strain curves were sampled between 0.020 and 0.200 MPa at an increment of 0.020 MPa. This sampling was the same for both axial and transverse strain data.

Results

Donor Demographics and Muscle Specimen Dimensions

In this study, pelvic floor complexes were obtained from 8 female human donors, for whom demographic information can be found in Table 1. Donor age ranged from 49 to 75 years, height from 1.52 to 1.68 m, and BMI from 19 to 33 kg/m^2 (Table 1). The mean age was 64.8 years, the mean height was 1.61 m, and the mean BMI was 25.4 kg/m^2. Due to the limited sample size, correlations and comparisons with demographic variables could not be made. As anticipated, dissection and mechanical testing techniques improved with each pelvic floor complex processed. We chose the mechanical testing order with this in mind, which explains the greater number of specimens obtained with increasing study identification number.

Table 2 depicts the mean ± standard deviation of specimen dimensions grouped by muscle. Within the SPMs, the TP specimens were the widest and thickest, while the IS specimens were the longest. It is worth noting that whole TP specimens were generally triangular in shape, with the medial end being noticeably wider than the lateral end. However, because our width measurements only considered areas that were predicted to be between the clamps, these whole muscle medial-lateral differences are not reflected in those data. LAM specimens were generally rectangular in shape, though that is not representative of LAMs in vivo and their size was much smaller than that of whole pubovisceralis or

iliococcygeus muscles. Even so, the LAM specimens were larger than SPM specimens (Table 2).

Load vs Displacement The axial load vs displacement for each muscle and specimen are depicted in Fig. 4. The individual load–displacement curves demonstrate that, overall, the LA and TP specimens covered a larger range of load values, reaching higher maximum loads than the BC or IS specimens (Fig. 4A). On average, the SPMs all exhibited similar load–displacement responses, stiffer than that of the LA specimens (Fig. 4B). Unsurprising given their greater initial length, the LAMs reached the largest displacement values, and exhibited the most compliant linear stiffnesses out of all muscle groups. The IS specimens had the greatest variability in stiffness and generally reached lower displacements than other muscles tested, likely due to their smaller initial size (Fig. 5).

Table 1 Donor demographics by individual with the quantity of muscle specimens tested

Study ID	Age (years)	Height (in)	BMI (kg/m2)	Quantity of BC specimens	Quantity of IS specimens	Quantity of TP specimens	Quantity of LA specimens
1	73	63	21	0	1	0	1
2	71	64	26	1	2	1	3
3	59	61	22	1	1	1	3
4	61	66	33	3	2	2	2
5	49	60	26	1	1	2	5
6	75	65	19	1	1	1	5
7	59	61	30	2	2	1	5
8	71	66	26	2	2	4	4

Table 2 Average dimensions of specimens tested in each muscle group. Data are presented as mean ± standard deviation

Muscle	N	Width (mm)	Thickness (mm)	Length (mm)	Gauge length (mm)
Bulbocavernosus	11	10.42 ± 2.38	3.67 ± 1.04	51.47 ± 10.13	23.96 ± 13.60
Ischiocavernosus	12	8.64 ± 2.28	3.66 ± 0.59	67.42 ± 14.95	37.08 ± 17.38
Transverse Perenei	12	12.71 ± 4.03	4.25 ± 1.27	45.06 ± 12.52	21.38 ± 8.65
Levator Ani	28	17.51 ± 5.79	3.86 ± 0.66	77.82 ± 17.59	51.46 ± 19.44

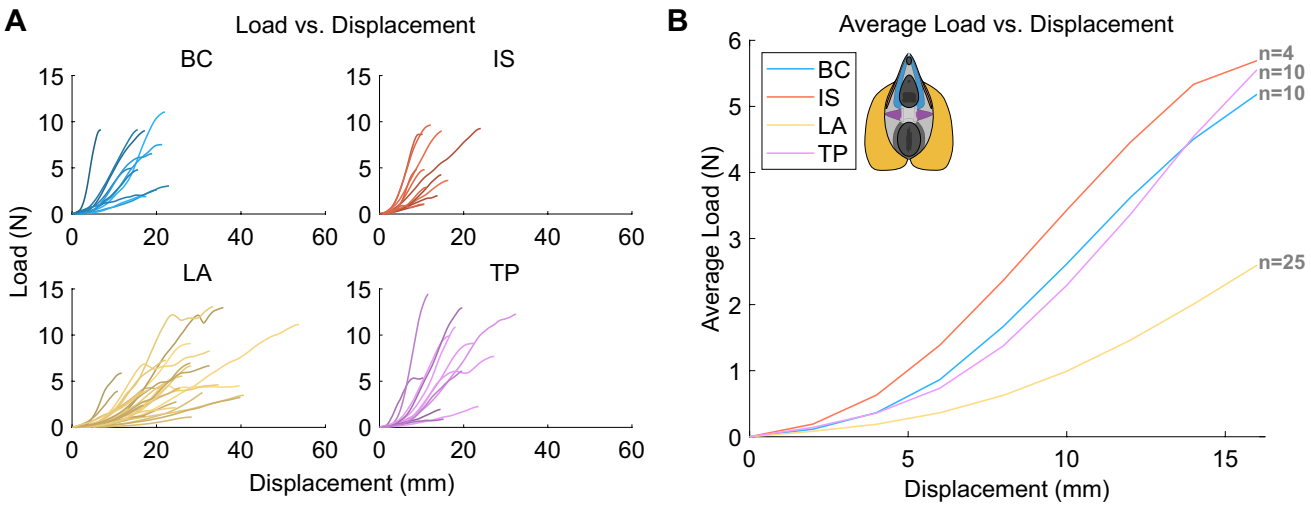

Fig. 4 Load vs displacement data. **A** Line plots grouped by muscle containing the continuous load–displacement curves for each individual specimen. **B** The average load–displacement data for each muscle group only including specimens that reached a displacement of 16 mm. Bulbocavernosus (BC), ischiocavernosus (IS), levator ani (LA), transverse perinei (TP).

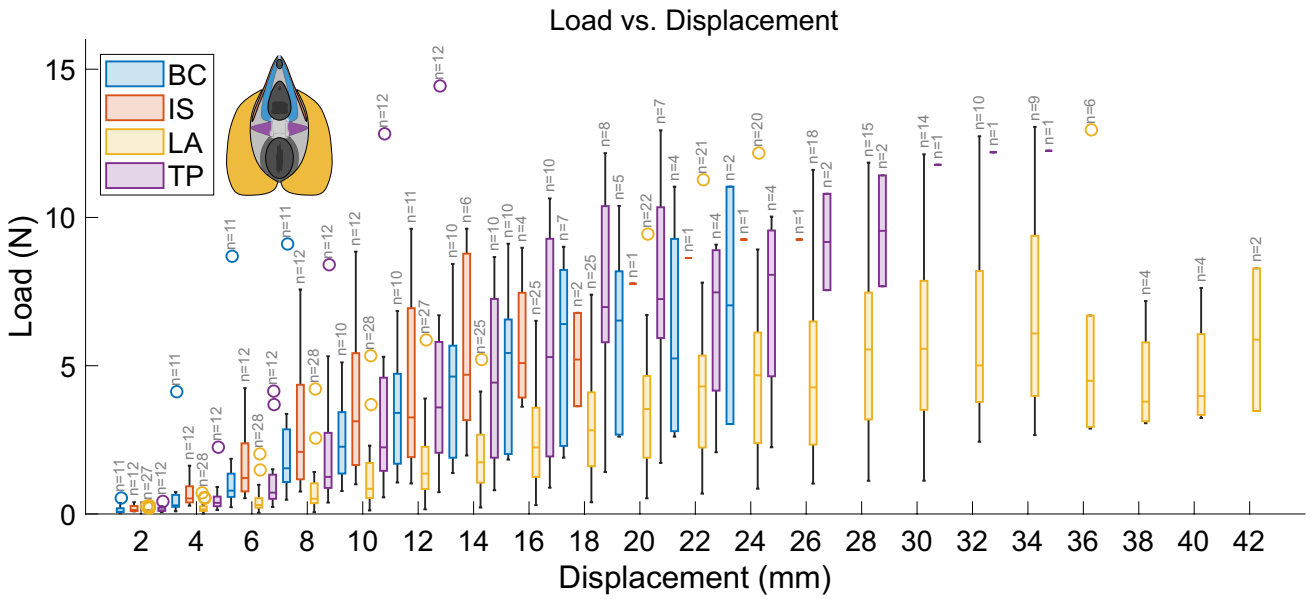

Fig. 5 Discrete load vs displacement data. Boxplots depicting load by muscle group at discrete displacement values. The sample size of each group decreases with increasing displacement as specimens failed or slipped and is indicated above each muscle group's data at each displacement value. Outliers are shown as empty circles. Bulbocavernosus (BC), ischiocavernosus (IS), levator ani (LA), transverse perinei (TP).

Stress vs Strain

Figure 6 depicts the stress vs axial strain data for the four muscle groups. Within each muscle group, the axial response varied dramatically from specimen to specimen, with some exhibiting a far stiffer response than others (Fig. 6A). There was more variation across the SPMs compared to the load–displacement data. Though the IS, on average, still had the stiffest behavior while the LA was still the most compliant, the average BC and TP curves fell in between the other two (Fig. 6B). The BC and TP average curves were the most similar, which was also the case with the load–displacement data. The TP exhibited the greatest range in axial strain values, with large variations in stress–strain data from specimen to specimen in both the small and large stress regions (Fig. 7). Within the small

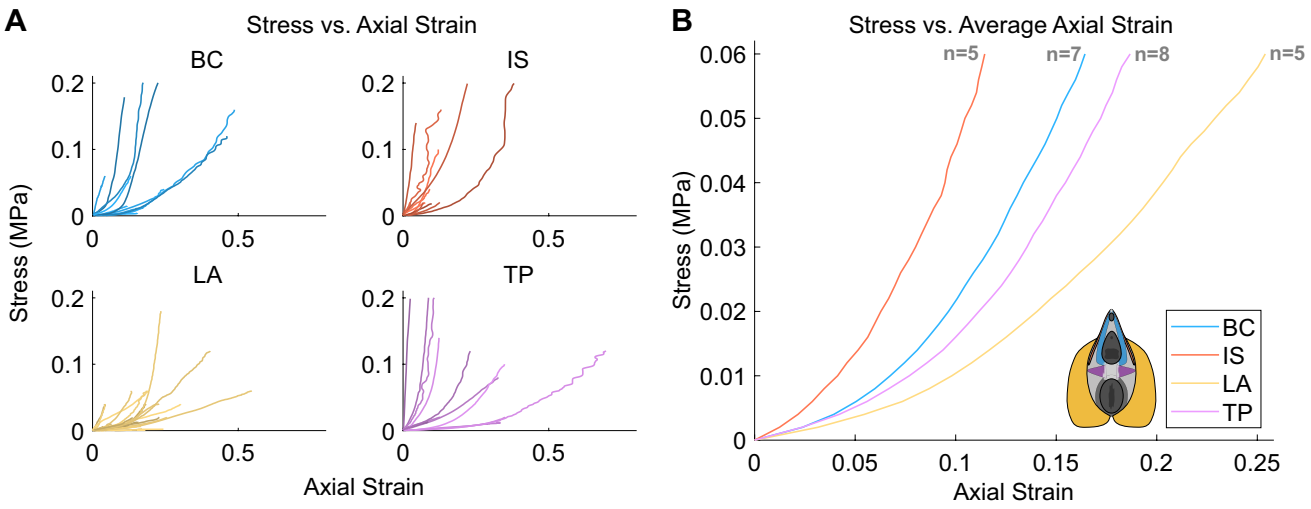

Fig. 6 Stress vs axial strain data. **A** Line plots grouped by muscle containing the continuous stress–axial strain curves for each individual specimen. **B** The average stress-axial strain data for each muscle group only including specimens that reached a stress of 0.06 MPa. Bulbocavernosus (BC), ischiocavernosus (IS), levator ani (LA), transverse perinei (TP).

stress region, the IS demonstrated the smallest amount of variability.

Figure 8 depicts the stress vs transverse strain data for each muscle group. In general, there was less variability between specimens of the same muscle group than that observed in the axial strain data. The LAM group had the fewest specimens reach stresses greater than 0.1 MPa (Fig. 8A). It is worth noting that some specimens experienced positive transverse strains, which has similarly been noted in previous studies that used DIC with uniaxial mechanical testing of fibrous biological tissues [21, 22]. This is possibly due to reorganization of collagen fibers in response to tensile loads. On average, LAM specimens experienced the greatest strains in the transverse direction with increasing stress, while the SPMs experienced comparable strains (Fig. 8B). These average curves reveal that, with regards to transverse strain, the SPMs behave remarkably similar while the LAMs are clearly distinct with transverse strain values that were roughly 2 to 3 times greater than those of the SPMs. The SPMs also exhibited a remarkably linear response in comparison to the LA's nonlinear average stress–transverse strain curve. When evaluating the discrete data, it is clear that the LAM demonstrated the greatest variability in transverse strains within the small stress region (Fig. 9). This trend continued in the large stress region until the LA group fell below an *n* of 3 at 0.08 MPa.

Discussion

This study is one of very few to evaluate the passive mechanical behavior of female human SPMs via ex vivo mechanical testing and to compare that to the still understudied LAMs; building upon a small amount of existing work focused on ex vivo mechanical testing of female human LAMs [12, 13]. Supporting our hypothesis, the LA on average demonstrated a response distinct from that of the SPMs. For example, at 0.06 MPa, LA axial and transverse strains were roughly 1.6× and 2.1× larger than average SPM strains. This suggests it is likely inappropriate to use LAM material properties and mechanical testing data to approximate and model the SPMs. This is particularly true when considering transverse strains, where the LA exhibited the most distinct behavior. It seems that utilizing muscle-specific mechanical data may even be important to consider within the SPMs, as stress–axial strain curves across the SPMs were distinct from one another. This further supports the need for appropriate, muscle-specific mechanical properties and more extensive data for these muscles.

While this is one of the first studies to evaluate the ex vivo passive mechanical behavior of female human SPMs, others have evaluated the LAMs. Burnett et al. evaluated the

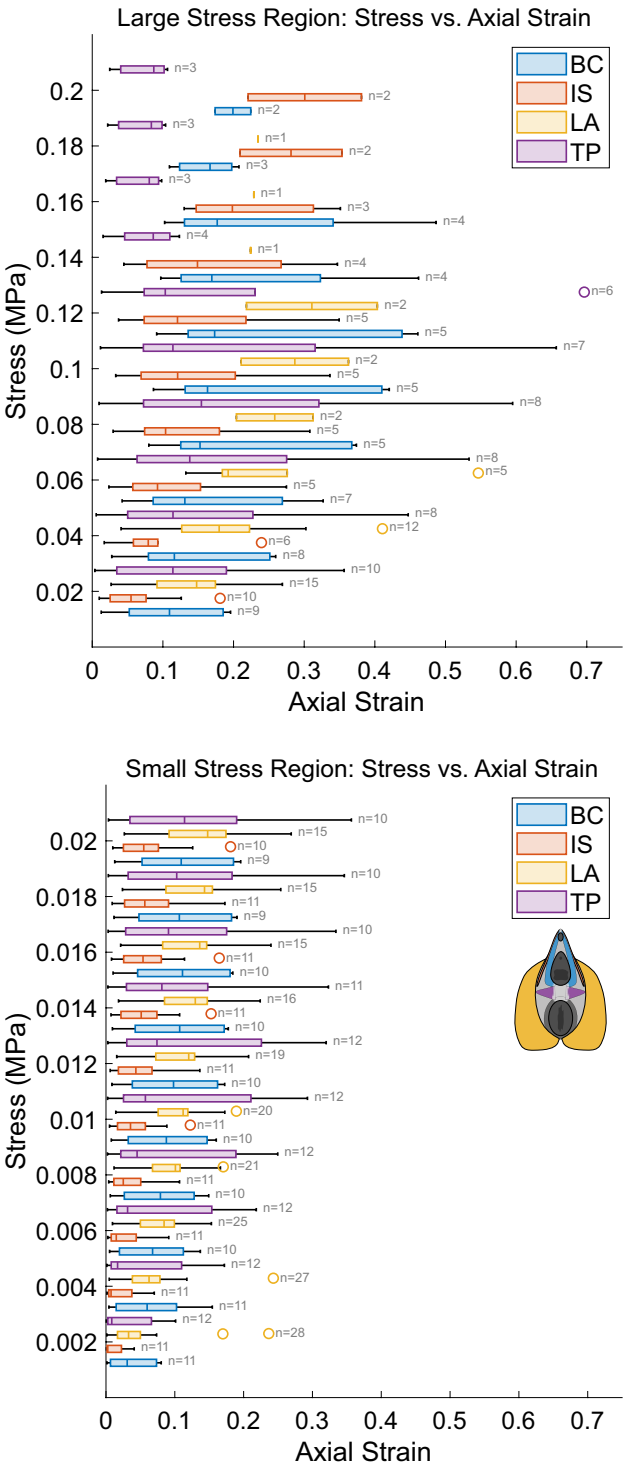

Fig. 7 Discrete stress vs axial strain data. Boxplots depicting axial strain by muscle group at discrete small and large stress values. The sample size of each group decreases with increasing stress as specimens failed or slipped, and is indicated next to each muscle group's data at each stress value. Outliers are shown as empty circles. Bulbocavernosus (BC), ischiocavernosus (IS), levator ani (LA), and transverse perinei (TP).

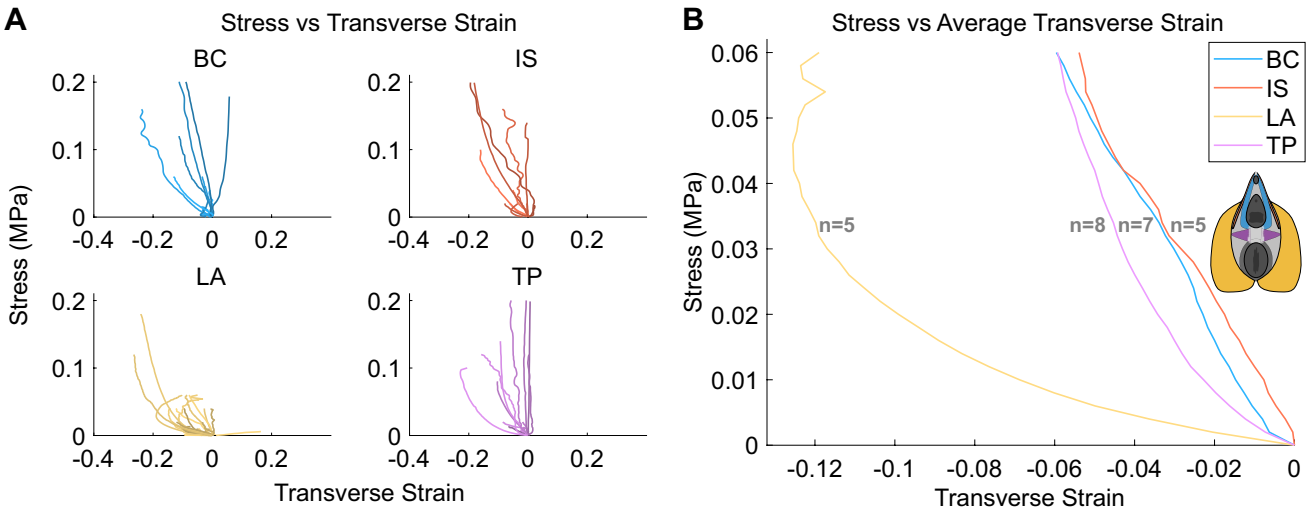

Fig. 8 Stress vs transverse strain data. **A** Line plots grouped by muscle containing the continuous stress–transverse strain curves for each individual specimen. **B** The average stress–transverse strain data for each muscle group only including specimens that reached a stress of 0.06 MPa. Bulbocavernosus (BC), ischiocavernosus (IS), levator ani (LA), and transverse perinei (TP).

passive mechanics of individual components of the LAMs and coccygeus muscles at the fiber bundle level. This study found that these pelvic floor muscles had similar stiffnesses to one another, but larger stiffnesses than those of the non-pelvic muscles tested [12]. Given that the specimens tested were at the bundle level, data cannot be directly compared to the present study. Although stress and strain are size independent, muscle fiber bundles and our muscle specimens represent different materials. For example, fiber bundles likely have a lower relative extracellular matrix content as they do not include the muscle's epimysium. Others have found that data must be scaled non-linearly to be able to compare muscle-scale and bundle-scale passive mechanics data [23]. The differences in axial LA stiffness between this study and previous studies could also be explained by the strain measurement method used. While existing studies estimated strain from clamp displacement, we utilized DIC to measure local strain fields across the surface of each specimen, noting that the strains varied heterogeneously (indicative of local variations in muscle composition).

In terms of size, LA specimens tested by Nagle et al. are more similar to those tested in this study; however, all donors in that study were postmenopausal and the average donor age was greater than that of our study (82.9 vs 64.8 years). Their average load–displacement curve demonstrates that specimens failed around 11 or 12 mm of displacement, while our study seemed to have many more specimens reach greater displacements before failing (Fig. 5). Additionally, at 12 mm of displacement our average load was less than 2 N while theirs was around 5 N, despite our study having larger LA specimens on average (specifically, a larger average width by 9.96 mm, larger average thickness by 0.86 mm, and larger average length by 38.24 mm) [13]. The greater compliance observed in the LA specimens in the present study may be the result of the younger average donor age. An increase in age (and weight) have previously been associated with an increase in stiffness in the LAMs, coccygeus muscles, and other pelvic tissues [12, 24]. Furthermore, weight and age have been identified as risk factors for the development of pelvic floor disorders [25, 26]. As donor medical history did not include whether any pelvic floor disorder symptoms were present before death, it is unknown whether any of the muscle specimens in this study were associated with pelvic floor dysfunction in vivo. Despite these differences between existing studies and the present study, each of the muscle groups tested exhibited nonlinear mechanical behavior and meaningful variability from specimen to specimen. These observations were also noted in the other human LAM ex vivo mechanical testing studies [12, 13]. Furthermore, stresses achieved by the LA during testing reasonably match those from these previous studies, with the muscle withstanding axial stresses up to tens to hundreds of kilopascals [12, 13].

Our study demonstrates that LAMs are consistently more compliant than SPMs, which may be indicative of differences in LAM and SPM structure and composition. This is supported to an extent by studies that have obtained histological images of portions of female human LAMs and SPMs that demonstrate differences between muscles [27, 28]; however, more robust and quantitative comparisons are still necessary. Additionally, some have looked at variation across different regions of the LA. Greater variability in muscle fiber size and larger connective tissue content (described as fibrosis) observed via histology were noted

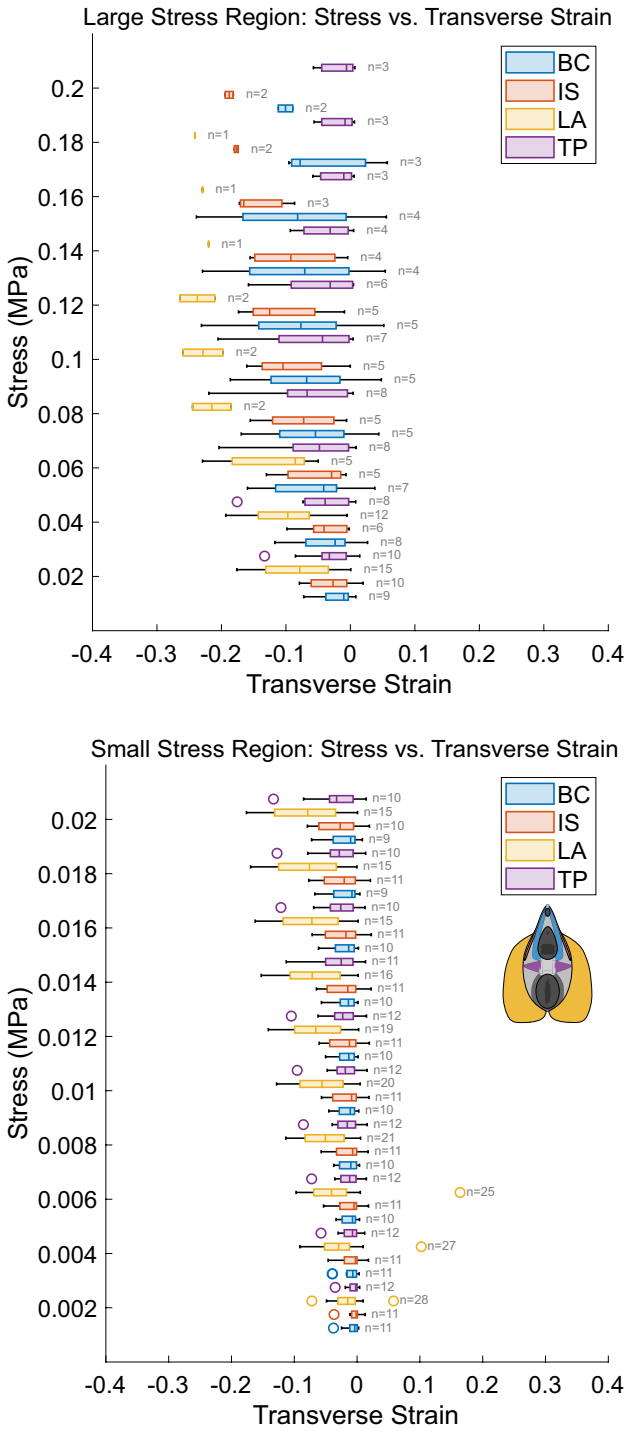

Fig. 9 Discrete stress vs transverse strain data. Boxplots depicting transverse strain by muscle group at discrete small and large stress values. The sample size of each group decreases with increasing stress as specimens failed or slipped and is indicated next to each muscle group's data at each stress value. Outliers are shown as empty circles. Bulbocavernosus (BC), ischiocavernosus (IS), levator ani (LA), and transverse perinei (TP).

in ventral regions of the LAM compared to dorsal regions [29]. These histomorphological features were even found to vary between the right and left sides, suggesting asymmetry in LA structure. These are examples of features of muscle composition that could be contributing both to variation within a muscle group and differences between the LAMs and SPMs. This likely difference in muscle structure is further supported by our own observations during this study. Only in LA specimens did we observe pockets of adipose tissue embedded between muscle fascicles and then tearing of those pockets before any noticeable muscle fiber tearing. This was not observed in any SPM specimen. These pockets of adipose tissue do not contribute to the LA specimen's effort to resist external tensile loads, which leads to compromised mechanical integrity and a more compliant stress–strain response. This could also explain the much larger transverse strains reached by the LA compared to the SPMs. LA specimens would compress laterally in response to tearing in those regions, eventually resulting in the collapse of these pockets of adipose tissue.

This study provides novel data characterizing the passive mechanical behavior of multiple female human SPMs and adds to existing LAM data, although it has several limitations. While a small sample size is common in human cadaveric studies, it reduces our ability to perform meaningful comparisons and draw conclusions representative of a broader, more inclusive population of female humans. Given that it was not always possible to obtain DIC strain data from specimens that we could obtain force–displacement data from, the stress–strain portion of our dataset in particular is limited by this. Future studies should investigate the impact of age, weight, other demographic variables, and pathology (such as pelvic organ prolapse) on the mechanical properties of the LAMs and SPMs. Additionally, we could not control what happened to the cadavers before we received them. It was not guaranteed that the obtained pelvises had only undergone one freeze-thaw cycle. Once dissected, tissues had to be frozen again until it was time for individual specimen dissection and mechanical testing. Thus, the time from death to initial freezing and number of freeze-thaw cycles may have influenced these data. However, studies have found freezing and refreezing to have a minimal impact on the passive stiffness of musculoskeletal tissues [30, 31]. Furthermore, any influence is expected to have impacted all donors and muscle specimens in this study similarly, thus not influencing comparisons made. The LAMs are larger than the SPMs, as such, there is inherently a greater ability to acquire testing specimens from different sub-regions of those muscles. We suspect that this type of variability impacted the LA data more than the SPM data; however, histological analyses were not performed to verify whether differences in mechanical properties correspond with differences in tissue structure and composition. We believe that

evaluating region-specific variability in LAM mechanical properties and correlating mechanical behavior with quantitative measures of tissue structure should be investigated in future studies. Finally, given the lack of existing SPM passive mechanics data, small amount of existing female human LAM data, and the fact that our tissues had to be frozen before mechanical testing, we decided on a simple uniaxial extension to failure protocol. Future studies could build upon this dataset by performing biaxial and viscoelastic mechanical testing and investigating heterogeneity across LAM subdivisions. That being said, this is still one of the only studies to evaluate the passive mechanical behavior of female human SPMs via ex vivo uniaixal mechanical testing and provides valuable data that will expand our knowledge of female pelvic floor biomechanics and advance the field of female pelvic medicine.

Acknowledgements The authors gratefully acknowledge the individuals who generously donated their or their loved one's bodies via the Anatomy Gifts Registry to support the advancement of science and medical research. We also thank the Office for Oversight of Anatomic Specimens at the University of Pittsburgh for making this study possible.

Author Contributions Conceptualization: M. Routzong and S. Abramowitch. Resources: M. Routzong, R. De Vita, P. Moalli, and S. Abramowitch. Methodology: M. Routzong, J. Dubik, R. De Vita, and S. Abramowtich. Investigation, Formal Analysis, and Software: M. Routzong and J. Dubik. Visualization: M. Routzong. Writing—Original Draft: M. Routzong and J. Dubik. Writing—Review and Editing: R. De Vita, M. Alperin, P. Moalli, and S. Abramowitch. All authors read and approved the final manuscript.

Funding This material is based upon work supported by the National Science Foundation Graduate Research Fellowship Program under Grant #1747452 (M. Routzong). S. Abramowitch, R. De Vita, and J. Dubik acknowledge support from the National Science Foundation Grant No. 2053851. Any opinions, findings, and conclusions or recommendations expressed in this material are those of the author(s) and do not necessarily reflect the views of the National Science Foundation. The authors acknowledge support from the Eunice Kennedy Shriver National Institute of Child Health & Human Development of the National Institutes of Health under Award Number K99HD115224 (M. Routzong) and NIH T32 HD007203 (M. Routzong). The content is solely the responsibility of the authors and does not necessarily represent the official views of the NICHD or NIH.

Data Availability The data supporting the findings of this study are available within the article. Reasonable requests for additional data or information can be made to the corresponding author.

Declarations

Conflict of interest M. Alperin receives an editorial stipend from Elsevier, Inc. All other authors declare that they have no conflict of interest.

Ethical Approval Prior approval was obtained for this cadaver study from the Committee for Oversight of Research and Clinical Training Involving Decedents (CORID, Application #933) at the University of Pittsburgh (Pittsburgh, PA). Institutional Review Board (IRB) approval was not required and no clinical trials were involved (clinical trial number: not applicable). The Anatomy Gift Registry's protocols are in accordance with the ethical standards of the University of Pittsburgh and adhere to the tenets of the Declaration of Helsinki. Donors are acquired in strict accordance with the Uniform Anatomical Gift Act (UAGA) and the National Organ Transplantation Act (NOTA), and informed consent is obtained from donor's legal next of kin or the donor themselves in all cases.

Consent for Publication Not applicable.

References

1. Alperin, M., T. Kaddis, R. Pichika, M. C. Esparza, and R. L. Lieber. Pregnancy-induced adaptations in intramuscular extracellular matrix of rat pelvic floor muscles. *Am. J. Obstet. Gynecol.* 215:210.e1-210.e7, 2016.
2. Alperin, M., D. M. Lawley, M. C. Esparza, and R. L. Lieber. Pregnancy-induced adaptations in the intrinsic structure of rat pelvic floor muscles. *Am. J. Obstet. Gynecol.* 213:191.e1-191.e7, 2015.
3. Rieger, M. M., M. Wong, L. A. Burnett, F. B. Sesillo, B. B. Baynes, and M. Alperin. Mechanisms governing protective pregnancy-induced adaptations of the pelvic floor muscles in the rat preclinical model. *Am. J. Obstet. Gynecol.* 226:708.e1-708.e13, 2022.
4. Routzong, M. R., P. Moalli, G. Rostaminia, and S. D. Abramowitch. Morphological Variation in the Pelvic Floor Muscle Complex of Nulliparous, Pregnant, and Parous Women. *Ann. Biomed. Eng.* 51(7):1461–1470, 2023.
5. Routzong, M. R., G. Rostaminia, P. A. Moalli, and S. D. Abramowitch. Pelvic floor shape variations during pregnancy and after vaginal delivery. *Comput. Methods Programs Biomed.* 194:105516, 2020.
6. Chan, S. S., R. Y. Cheung, K. W. Yiu, L. L. Lee, and T. K. Chung. Effect of levator ani muscle injury on primiparous women during the first year after childbirth. *Int. Urogynecol. J.* 25:1381–1388, 2014.
7. Fairchild, P. S., L. K. Low, K. M. Kowalk, G. E. Kolenic, J. O. DeLancey, and D. E. Fenner. Defining "normal recovery" of pelvic floor function and appearance in a high-risk vaginal delivery cohort. *Int. Urogynecol. J.* 31:495–504, 2020.
8. Handa, V. L., J. L. Blomquist, L. R. Knoepp, K. A. Hoskey, K. C. McDermott, and A. Muñoz. Pelvic floor disorders 5–10 years after vaginal or cesarean childbirth. *Obstet. Gynecol.* 118:777, 2011.
9. Memon, H. U., and V. L. Handa. Vaginal childbirth and pelvic floor disorders. *Women's Health* 9(3):265–277, 2013.

10. Pessoa, P., A. Carvalho, and P. Mota. Prevalence of levator ani muscle injuries in primiparous women after delivery and their influence on pelvic floor disorders-systematic review. *Neurourol. Urodyn.* 43(8):1962–1969, 2024.
11. Kenne, K. A., L. Wendt, and J. B. Jackson. Prevalence of pelvic floor disorders in adult women being seen in a primary care setting and associated risk factors. *Sci. Rep.* 12:9878, 2022.
12. Burnett, L. A., M. Cook, S. Shah, M. M. Wong, D. M. Kado, and M. Alperin. Age-associated changes in the mechanical properties of human cadaveric pelvic floor muscles. *J. Biomech.* 98:109436, 2020.
13. Nagle, A. S., M. A. Barker, S. D. Kleeman, B. Haridas, and T. Douglas Mast. Passive biomechanical properties of human cadaveric levator ani muscle at low strains. *J. Biomech.* 47:583–586, 2014.
14. Zifan, A., M. Reisert, S. Sinha, M. Ledgerwood-Lee, E. Cory, R. Sah, and R. K. Mittal. Connectivity of the superficial muscles of the human perineum: a diffusion tensor imaging-based global tractography study. *Sci. Rep.* 8:17867, 2018.
15. DeLancey, J. O. Anatomie aspects of vaginal eversion after hysterectomy. *Am. J. Obstet. Gynecol.* 166:1717–1728, 1992.
16. Routzong, M. R., P. A. Moalli, S. Maiti, R. De Vita, and S. D. Abramowitch. Novel simulations to determine the impact of superficial perineal structures on vaginal delivery. *Interface Focus.* 9:20190011, 2019.
17. Moura, R., D. A. Oliveira, M. P. Parente, N. Kimmich, and R. M. N. Jorge. A biomechanical perspective on perineal injuries during childbirth. *Comput. Methods Programs Biomed.* 243:107874, 2024.
18. Lionello, G., C. Sirieix, and M. Baleani. An effective procedure to create a speckle pattern on biological soft tissue for digital image correlation measurements. *J. Mech. Behav. Biomed. Mater.* 39:1–8, 2014.
19. Abramowitch, S., and D. Easley. Introduction to classical mechanics. In: Biomechanics of the female pelvic floor, Elsevier, 2016, pp. 89–107.
20. Lake, S. P., J. G. Snedeker, V. M. Wang, H. Awad, H. R. Screen, and S. Thomopoulos. Guidelines for ex vivo mechanical testing of tendon. *J. Orthopaedic Res.®*. 41:2105–2113, 2023.
21. Donaldson, K., and R. De Vita. Ex vivo uniaxial tensile properties of rat uterosacral ligaments. *Ann. Biomed. Eng.* 51:702–714, 2023.
22. Mallett, K. F., and E. M. Arruda. Digital image correlation-aided mechanical characterization of the anteromedial and posterolateral bundles of the anterior cruciate ligament. *Acta Biomater.* 56:44–57, 2017.
23. Ward, S. R., T. M. Winters, S. M. O'Connor, and R. L. Lieber. Non-linear scaling of passive mechanical properties in fibers, bundles, fascicles and whole rabbit muscles. *Front. Physiol.* 11:211, 2020.
24. Baah-Dwomoh, A., J. McGuire, T. Tan, and R. De Vita. Mechanical properties of female reproductive organs and supporting connective tissues: A review of the current state of knowledge. *Appl. Mech. Rev.* 68:060801, 2016.
25. MacLennan, A. H., A. W. Taylor, D. H. Wilson, and D. Wilson. The prevalence of pelvic floor disorders and their relationship to gender, age, parity and mode of delivery. *BJOG.* 107:1460–1470, 2000.
26. Hendrix, S. L., A. Clark, I. Nygaard, A. Aragaki, V. Barnabei, and A. McTiernan. Pelvic organ prolapse in the women's health initiative: gravity and gravidity. *Am. J. Obstet. Gynecol.* 186:1160–1166, 2002.
27. Muro, S., L. Chang, S. Tharnmanularp, A. Nimura, H. Churei, and K. Akita. Presence of smooth muscle continuous with the rectal and vaginal walls in the deep perineal space prompts reconsideration of the deep transverse perineal muscle. *Sci. Rep.* 15:23730, 2025.
28. Stein, T. A., and J. O. DeLancey. Structure of the perineal membrane in females: gross and microscopic anatomy. *Obstetr. Gynecol.* 111:686–693, 2008.
29. Jundt, K., M. Kiening, P. Fischer, F. Bergauer, E. Rauch, W. Janni, U. Peschers, and T. Dimpfl. Is the histomorphological concept of the female pelvic floor and its changes due to age and vaginal delivery correct? *Neurourol. Urodyn.* 24:44–50, 2005.
30. Van Ee, C., A. Chasse, and B. Myers. Quantifying skeletal muscle properties in cadaveric test specimens: effects of mechanical loading, postmortem time, and freezer storage. *J. Biomech. Eng.* 122:9–14, 2000.
31. Moon, D. K., S. L. Woo, Y. Takakura, M. T. Gabriel, and S. D. Abramowitch. The effects of refreezing on the viscoelastic and tensile properties of ligaments. *J. Biomech.* 39:1153–1157, 2006.